ISSN 0145-8752, Moscow University Geology Bulletin, 2010, Vol. 65, No. 1, pp. 39–48. © Allerton Press, Inc., 2010.
Original Russian Text © N.V. Chertkova, A.E. Tsai, N.L. Mironov, V.D. Shcherbakov, 2010, published in Vestnik Moskovskogo Universiteta. Geologiya, 2010, No. 1, pp. 39–47.

Thermodynamic Settings of Melting and Melt Ascent from Magmatic Chambers Using the Example of Klyuchevskoi Volcano

N. V. Chertkova[a], A. E. Tsai[a], N. L. Mironov[b], and V. D. Shcherbakov[a]

[a] *Department of Petrology, Faculty of Geology, Moscow State University, Moscow, Russia*
e-mail: nvchertkova@gmail.com; sasha-msu@yandex.ru; vasiliy7@gmail.ru
[b] *Vernadsky Institute of Geochemistry and Analytical Chemistry, Russian Academy of Sciences, Moscow, Russia*
e-mail: nikita_mir@rambler.ru

Received April 14, 2009

Abstract—Theoretical models and experimental data on the thermodynamic and rheological properties of basalts from the Apakhonchich lava flow (Klyuchevskoi Volcano, Kamchatka) were invoked for plotting projections of water-containing and dry liquidus and solidus curves on the P_s–T plane. The P–T–X_{H_2O} conditions for the formation of basaltic magma and the degree of its differentiation were determined from data on melt inclusions. The calculated apparent viscosity of the melt containing 10% crystals at 1100°C, 1 GPa, and 3 wt % water is 1.1×10^3 Pa s, and the density is 2.5 g/cm^3.

Key words: thermodynamics of basalt solidus and liquidus, viscosity, Klyuchevskoi Volcano.
DOI: 10.3103/S0145875210010047

LEGEND

Phases: Ol_g, olivine and its generations (I, II, III), $Ol_{Fo\,82}$, where the subscript index $Fo = 100 \times Mg/(Mg + Fe^{2+})$; *Cpx*, clinopyroxene; *Pl*, plagioclase.

Thermodynamic indices: M_i, molecular weight of the ith component; M^{liq}, melt molecular weight; P, total pressure of the gaseous fluid; P_{H_2O}, partial pressure of water in the fluid; P_S, pressure experienced by crystals and the melt, or lithostatic pressure; $S^{fl}_{H_2O}$, entropy of water in the fluid; S^{liq}, entropy of dry basalt melt; S^{sol}, entropy of solid basalt; t, temperature, °C; T, temperature, K; $V^{liq}_{H_2O}$, water volume in the fluid; V^{liq}, volume of dry basalt melt; V^{sol}, volume of solid basalt; X_i, molar fraction of the ith component in a given phase; $\mu^{liq}_{K_2O}$, chemical potential of potassium oxide; X^{liq}_i and N^{liq}_i, the molar fraction and weight percentage of the ith component in the melt, respectively.

INTRODUCTION

Current knowledge of the conditions under which rocks of different composition melt and crystallize is sufficient for solving certain problems concerning the mobility of silicic melts in the Earth's crust and the thermodynamic conditions of their solidification on the surface. It is known that melting and melt crystallization depend not only on temperature and pressure, but also on the presence of volatile components and their oxidation levels (f_{O_2}). The degree of rock crystallinity can vary within a broad range in each lava flow of any volcano, and this range is determined not so much by the endogenous parameters as the conditions of effusion and formation of the flow.

Study of the gaseous phase produced by eruptions has shown that the major volatile components of magmatic melts are water and carbon dioxide. Statistical analysis is indicative of the predominant role of water in the gaseous phases of volcanoes located at the junctures of lithospheric plates [Mysen, 2004]. It follows from experimental data that carbon dioxide is very little soluble in silicic melts at pressures below 1 GPa: in basaltic melts N_{CO_2} is below 0.06 wt % at $P < 100$ MPa and below 0.9 wt % at $P < 1$ GPa and 1200°C $< t <$ 1400°C [Dixon et al., 1995]. However, carbon dioxide solubility at pressures about 2 GPa depends significantly on the degree of melt polymerization and contents of bases, i.e., on melt composition [Holloway et al., 1976; Persikov, 1984]. Under P–T conditions characteristic of eruptions, the water content in the melt has the most significant influence on the degree of crystallization of magma during its ascent to the surface.

During the second half of the 20th century, ample information was obtained on water solubility in melts

of some minerals, for example, [Silver and Stolper, 1985], and rocks [Kadik, 1971]. The combined effect of total pressure and f_{O_2} on the crystallization of water-saturated basalt melt at 1100°C was studied by Hamilton et al. [1964]. The following water solubility values were obtained: 3.1 wt % at $P_{H_2O} = 100$ MPa and 9.4 wt % at $P_{H_2O} = 600$ MPa. In these studies, the effects of oxygen fugacity f_{O_2} on the order of phase crystallization and liquidus temperature (T^{liq}) of basalt were demonstrated. At high f_{O_2} values (buffer Fe_2O_3–Fe_3O_4), T^{liq} exceeded 1230°C, and at low f_{O_2} (buffer FeO–Fe_2O_3), $T^{liq} = 1020$°C at $P_S = 100$ MPa.

Less data are available on melts that are undersaturated with water. The most detailed information on water solubility on the basaltic melt liquidus curve at $P_{H_2O} \le P_S$ below 2 GPa was presented by Perchuk [1985]. It allows construction of water solubility contour lines for melts undersaturated with water on the P–T plane. Therefore, we invoked this information for further thermodynamic constructions.

Water content in magmatic melts should be taken into account in evaluation of melt transport properties, i.e., viscosity. The most detailed results of experimental studies of silicic melt viscosity are summarized in the model constructed by Persikov [1984, 1991]. This model is based on Ya. Frenkel's kinetic theory of liquids and theoretical consideration of the relationship between the structures of magmatic melts and their compositions. The model provides accurate calculations and predictions of the rheological properties of melts depending on temperature, fluid pressure, total pressure, contents of rock-forming and volatile components, and volumes of crystals and bubbles in the magma.

We applied theoretical methods to basalt samples from lava flows of Klyuchevskoi Volcano in the context of available experimental data on basalt melting, water solubility, and melt viscosity. The objectives of our work were: (1) construction of melting curves in P_S–T coordinates, including construction of dry and water-saturated solidus curves and water solubility contour lines, for the basalt sample under study; (2) determination of the trend of its evolution in the P–T–X_{H_2O} coordinates; and (3) evaluation of magma viscosity and its transport properties.

METHODS

The P–T parameters of the liquidus and solidus curves were determined from their dependence on the compositions of the rock and the liquidus phase [Perchuk, 1983; Ariskin, 1999]. Contour lines of water solubility and water pressure were constructed on the basis of thermodynamic equations [Perchuk, 1973; *Petrografiya*, 1976] and experimental data reported in [Hamilton et al., 1964; Nesbit and Hamilton, 1970; Burnham and Davis, 1971; Perchuk, 1985]. The P–T trend of basalt melt evolution was filled in the basalt fusibility chart with assessments of water contents at particular stages based on examination results of melt inclusions [Mironov et al., 2001; Mironov and Portnyagin, 2008]. Basalt melt viscosity was calculated according to E.S. Persikov's model [Persikov, 1984; 1991]. The combined use of these methods allows one to solve modern tasks concerning magmatic melt formation and evolution.

PETROGRAPHY

The theoretical analysis of the thermodynamic settings of basalt evolution was performed by the example of a sample from the Apakhonchich lava flow, Klyuchevskoi Volcano [Mironov et al., 2001]. The flow occurred on October 23, 1946, on the southeastern slope of the volcano at an elevation of 1500 m. The eruption gave rise to a block lava flow in the form of a narrow band effusing from a cinder cone. The flow consists of high-alumina basalt (Table 1). It contains phenocrysts of olivine (*Ol*), clinopyroxene (*Cpx*), and plagioclase (*Pl*). Plagioclase is predominant, and the amounts of *Cpx* and *Ol* vary in broad ranges and increase toward the bottom portions of the lavas flow. The amount of phenocrysts averaged over the flow is about 10%.

The best studied basalt sample, Ap-60-31, was chosen for theoretical analysis. It has a porphyric texture and the interstitial structure of the groundmass (Fig. 1a). Three generations were recognized according to the compositions of phenocrysts and melt inclusions in olivine [Mironov and Portnyagin, 2008] (Table 2): (1) the highest-magnesium olivine phenocrysts ($Ol_{Fo>82}$), which are products or early crystallization products with equilibrium melt inclusions containing 49.83 wt % SiO_2 and 11.32 wt % MgO; (2) varieties with lower magnesium contents ($Ol_{Fo\,82–73}$), whose melt inclusions contain 52.68 wt % SiO_2 and 4.43 wt % MgO; (3) ferruginous olivines ($Ol_{Fo<73}$) with inclusions of compositions close to andesite, indicative of their incorporation at the final stage.

The zoning characteristic of most plagioclase phenocrysts is shown in Fig. 2. The content of the anorthite component in phenocryst cores is constant, about 80 mol %. Tunnel dissolution structures and melt and gas inclusions are typical of central parts of the phenocrysts. The rim is about 100–150 μm thick. It contains less anorthite component, 55 mol %. The zoning typical for plagioclase phenocrysts is indicative of multistage rock evolution. There are various interpretations of the magmatic history of the formation of phenocrysts with such zoning. For example, Vance

Table 1. The chemical and normative compositions of the Klyuchevskoi Volcano basalt and adamellite

Component	Basalt**	Adamellite***	CIPW, wt %	Basalt	Adamellite
SiO_2	53.26	64.32	*Qtz*	0.00	17.77
TiO_2	1.08	1.20	*Or*	6.74	24.41
Al_2O_3	17.52	17.67	*Ab*	27.50	29.79
FeO*	8.55	5.51	*An*	29.85	9.23
MnO	0.16	0.11	*Fa*	0.53	0.00
MgO	5.62	1.67	*Fo*	0.47	0.00
CaO	8.45	1.86	*En*	10.87	4.16
Na_2O	3.25	3.52	*Fs*	11.03	8.34
K_2O	1.14	4.13	*Wol*	5.04	0.00
Total	99.03	100.00	*Di*	2.46	0.00
			Hyp	2.50	0.00
			Crn	0.00	4.03
			Ilm	2.05	2.28

Note: *, total iron content; **, average composition of high-alumina Apakhonchich basalts from A. P. Khrenov's collection; ***, composition of the residual melt after equilibrium crystallization of the basalt to 78 wt %.

[1965] explains the presence of the calcium core and sodium-enriched rim by the existence of two intermediate chambers at different depths. In Karymsky Volcano, plagioclases of a similar zoning are formed of mixing contrasting magmas [Izbekov et al., 2002].

Parageneses of phenocryst minerals are recognized according to solid-phase inclusions in *Ol*, *Cpx*, and *Pl*. The early generation (I) includes crystals and glomeroporphyric clots of *Ol* and *Cpx*, where the latter is clearly preponderant. In general, minerals of generation I are larger than later phenocrysts: from about 0.7–1 to 2–3 mm. The next generation (II) includes phenocrysts of *Ol, Cpx*, and *Pl* of ~0.5–1 mm in size. Generation III includes microphenocrysts of *Ol, Cpx,* and *Pl*, ~0.3–0.7 mm in size.

The basalt groundmass consists of microlites of plagioclase, pigeonite, titanomagnetite, and highly silicic glass (68–71 wt % SiO_2). Glass with microlites constitutes about 65% of the rock, and phenocrysts of generations I and II, no more than 10% (*Ol* > 1%, *Cpx* ~ 6%, and *Pl* ~ 3–4%). Mesophenocrysts of generation III constitute no more than 25% of the thin section. Of them, 20% are constituted of *Pl*, and 2–3%, of each of *Ol* and *Cpx*.

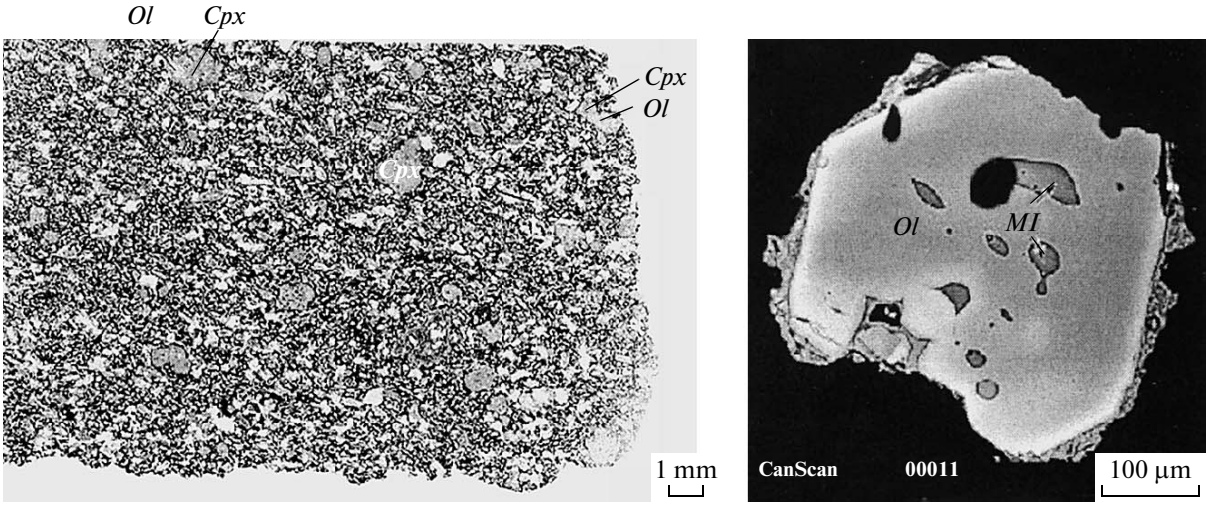

Fig. 1. Microstructures of (a) basalt (sample Ap-60-31) with large phenocrysts and glomeroporphyric intergrowths of olivine and clinopyroxene and (b) an olivine phenocryst with melt inclusions (*MI*) [Mironov et al., 2001]. Microphotographs were made: (a) with parallel nicols; (b) in back-scattered electron image.

Table 2. Chemical composition of melt inclusions in phenocryst minerals and calculation of T–P–N_{H_2O} [Mironov et al., 2001; Mironov and Portnyagin, 2008]

Composition	Generation					
	I		II	III		
	Ol	*Ol*	*Ol*	*Ol*	*Cpx*	*Pl*
SiO_2	49.83	50.09	52.68	55.77	55.06	55.36
TiO_2	0.81	0.98	1.20	1.56	1.39	1.53
Al_2O_3	14.14	16.71	18.14	15.33	16.17	15.53
FeO*	8.50	8.50	9.36	10.74	9.63	10.14
MnO	0.10	0.12	0.15	0.14	0.02	0.14
MgO	11.32	8.42	4.43	3.61	4.02	4.09
CaO	11.99	11.07	8.80	6.79	7.60	7.64
Na_2O	2.42	3.08	3.87	4.12	4.12	3.98
K_2O	0.59	0.74	1.04	1.60	1.27	1.44
P_2O_5	0.14	0.17	0.20	0.25	–	–
Ni	90.0	86.7	77.7	70.9	72.4	61.21
N_{H_2O}, wt %	3.3	3.9	3.8	2.0		
Standard deviation	0.1	0.4	1.3	1.0		
P, GPa	1.08	0.79	0.36	0.28		
Standard deviation	2.6	2.7	2.3			
T, °C	1243	1149	1028	1068		
Standard deviation	28	64	48	37		
n	5	27	34	5	14	2

Note: *Ni*, mol %, where $i \sim Fo = 100Mg/(Mg + Fe^{2+})$ for olivine; $\sim Mg\# = 100Mg/(Mg + Fe^{2+})$ for clinopyroxene; $\sim An = 100Ca/(Ca + Na)$ for plagioclase; and n, the number of inclusions.

The construction of the projections of basalt liquidus and solidus curves onto the P_s–T plane: the liquidus. The dry liquidus for sample Ap-60-31 was constructed from experimental data [Perchuk, 1983, 1985] to P_s = 1 GPa. At P_s = 1 atm, the calculated melting temperature was 1208°C, and $(dP/dt)^{liq} \approx 25$ MPa/°C. Earlier, it was suggested that basalt composition did not affect the solubility of water in the melt [Perchuk, 1973]. Experimental data on the liquidus in the alkali basalt–water system were obtained later [Perchuk, 1985].

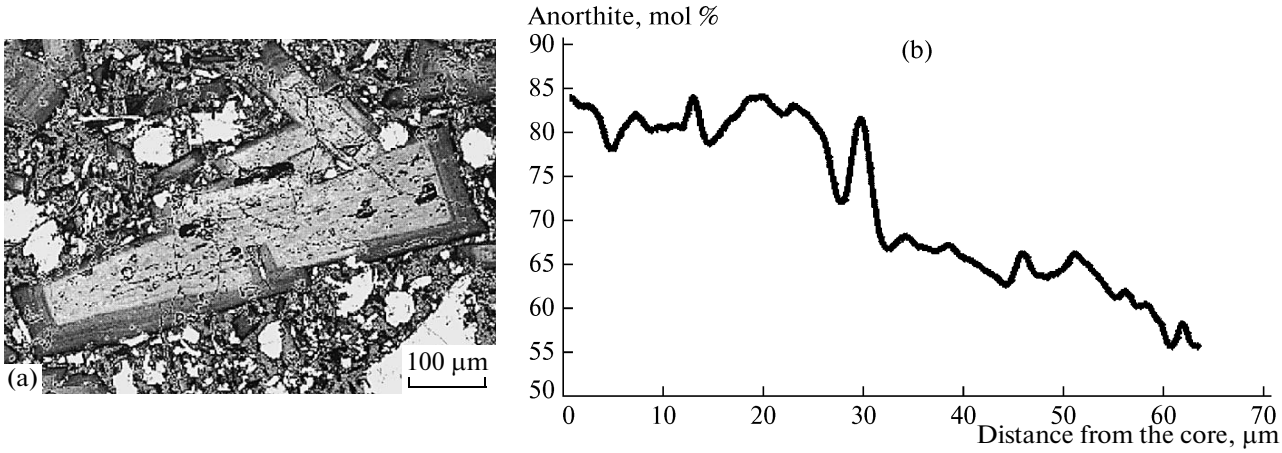

Fig. 2. (a) Microphotograph of a plagioclase phenocryst in back-scattered electrons; (b) its zoning from the core to the edge.

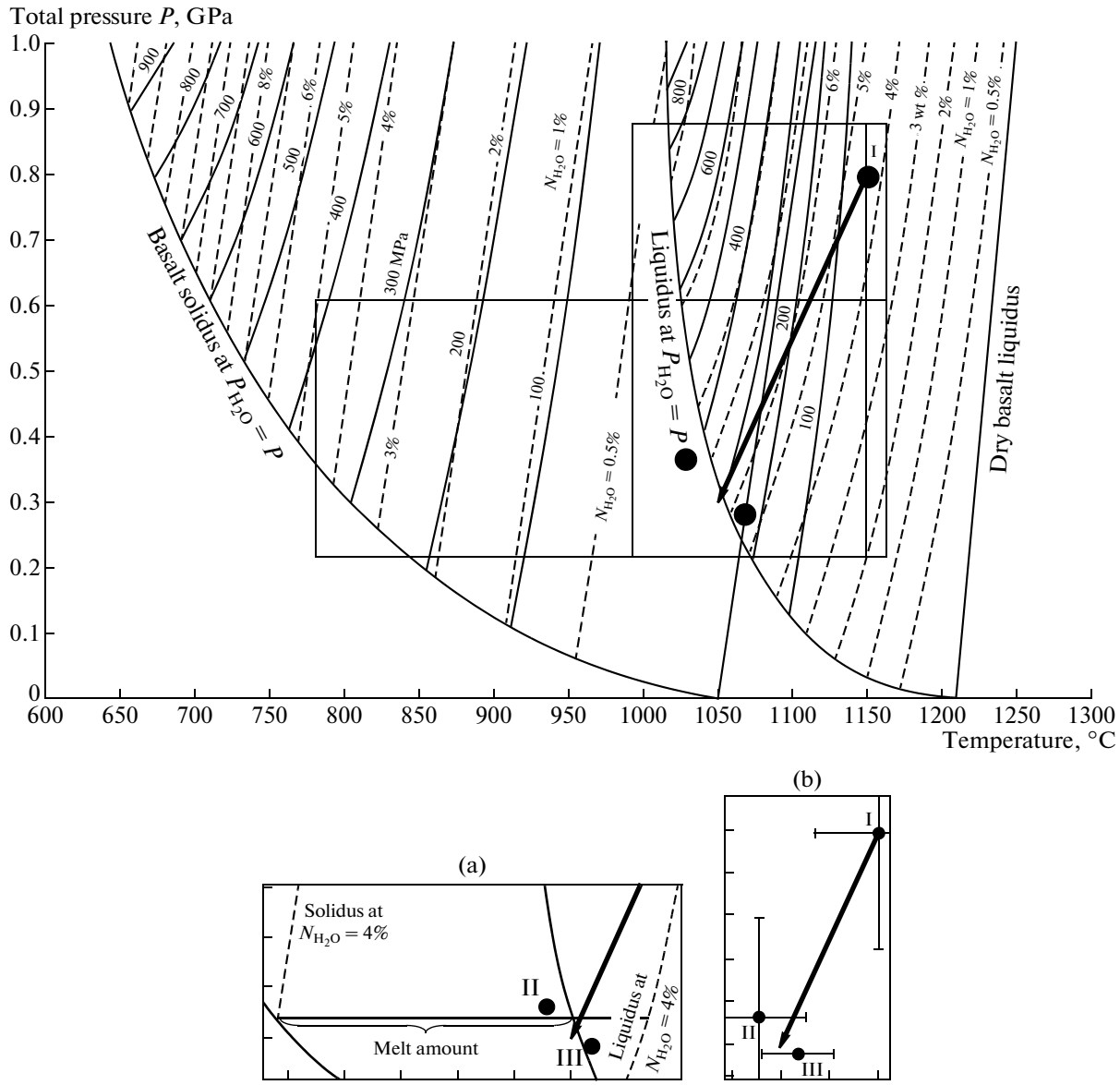

Fig. 3. *P–T* melting diagram of high-alumina basalt from the Apakhonchich lava flow, Klyuchevskoi Volcano. Solid lines are projections of the basalt liquidus and solidus at preset water concentrations (P_{H_2O}, MPa). Dashed lines are contour lines of equal water content (wt %) on the melt liquidus. Black circles are mean values of *P–T* parameters determined from melt inclusions [Mironov et al., 2001; Mironov, Portnyagin, 2008]. Arrow: the *P–T* trend of melt evolution during its ascent to the surface. (a) ratio between the liquid and crystalline phases at 4 wt % water in the melt and the *P–T*-crystallization parameters of olivine generations II and III; (b) error of *P–T* parameters evaluation from melt inclusions.

We compared these data with those predicted from the thermodynamic consideration of previous results [Hamilton et al., 1964; Nesbit and Hamilton, 1970] to the pressure of 1 GPa. According to the latter results, the dependences of P and t on N_{H_2O} are described by the following equations [Perchuk, 1973]:

$$t(^\circ\mathrm{C}) = 1167.08 - 32.43N_{H_2O} + 2.46N_{H_2O}^2 - 0.07N_{H_2O}^3, \quad (1)$$

$$P(\mathrm{MPa}) = 100(-806.26 + 626.73N_{H_2O} + 18.69N_{H_2O}^2 - 0.43N_{H_2O}^3), \quad (2)$$

where N_{H_2O} is water concentration in the melt, wt %.

The water-saturated liquidus curve constructed from these equations (Fig. 3) and the dry liquidus curve constructed for the basalt sample under study are in good agreement with the experimental data for the alkali basalt–water system [Perchuk, 1985]. Hence,

Table 3. Molecular weights, volumes, and densities of the basalt and adamellite melts

Component	Basalt						Component	Adamellite					
	wt %	m_i	X_i	M_iX_i	according to [Appen, 1970]			wt %	m_i	X_i	M_iX_i	according to [Appen, 1970]	
					V_t^{liq}	$X_iV_t^{liq}$						V_t^{liq}	$X_iV_t^{liq}$
SiO_2	53.26	0.89	0.57	34.41	26.70	15.29	SiO_2	64.32	1.07	0.71	42.53	26.70	18.90
TiO_2	1.08	0.01	0.01	0.70	20.60	0.18	TiO_2	1.20	0.01	0.01	0.79	20.60	0.20
Al_2O_3	17.52	0.17	0.11	11.32	40.40	4.49	Al_2O_3	17.67	0.17	0.11	11.68	40.40	4.63
FeO	8.55	0.12	0.08	5.52	16.50	1.27	FeO	5.51	0.08	0.05	3.64	16.50	0.84
MnO	0.16	0.00	0.00	0.10	15.00	0.02	MnO	0.11	0.00	0.00	0.07	15.00	0.02
MgO	5.62	0.14	0.09	3.63	12.50	1.13	MgO	1.67	0.04	0.03	1.11	12.50	0.34
CaO	8.45	0.15	0.10	5.46	14.40	1.40	CaO	1.86	0.03	0.02	1.23	14.40	0.32
Na_2O	3.25	0.05	0.03	2.10	20.20	0.68	Na_2O	3.52	0.06	0.04	2.33	20.20	0.76
K_2O	1.14	0.01	0.01	0.74	34.10	0.27	K_2O	4.13	0.04	0.03	2.73	34.10	0.99
Total	99.03	1.55	1.00	63.99		24.73	Total	100.00	1.51	1.00	66.12		26.99
Basalt melt density 2.75 g/cm^3							Adamellite melt density 2.68 g/cm^3						

Note: m_i, atomic amount; V_t^{liq}, partial molar volume of the oxide in the melt [Appen, 1970].

they can be used for constructing the water-saturated liquidus curve and contour lines of water solubility in the melt for Klyuchevskoi Volcano.

The equilibrium melting of basalt is described by the following equation [Perchuk, 1973]:

$$(1-x)\ \text{basalt} + x\text{H}_2\text{O} = x\text{H}_2\text{O}(1-x)\ \text{melt}, \quad (3)$$

where x is the molar fraction of water in the melt.

If the system is closed ($P_{\text{H}_2\text{O}} = P$), variation in T and P will result in a shift of the eutectic point along monovariant curve (1) to the low-temperature area. This shift is described by Eq. (4):

$$\frac{dP_{\text{H}_2\text{O}}}{dT} = \frac{S^{liq} - xS^{fl}_{\text{H}_2\text{O}} - (1-x)S^{sol}}{V^{liq} - xV^{fl}_{\text{H}_2\text{O}} - (1-x)V^{sol}} = \frac{\Delta S_{(1)}}{\Delta V_{(1)}}. \quad (4)$$

Projections of the basalt liquidus curve on the P_S–t plane at specified $P_{\text{H}_2\text{O}}$ values were calculated by the method described by Perchuk [1973]. The results of calculation of molecular weight (M_i), volume (V^{sol}), and density (ρ) for the dry basalt melt from the Apakhonchich lava flow are shown in Table 3. The volume effect (ΔV) can be calculated by assuming $V^{sol} = \Sigma X_iM_i/\rho = 23.24$, and then $V^{liq} - V^{sol} = \Delta V = 1.49$ cm^3 to the pressure 1 GPa. From the volume effect and $(dP/dt)^{liq}$, the entropy effect ΔS of basalt melting can be calculated:

$$\Delta S = \Delta V(dP/dt)^{liq}$$
$$= 37.259\ \text{cm}^3\text{MPa}/^\circ\text{C} = 8.91\ \text{e.u.}$$

At specified $P_{\text{H}_2\text{O}}$ values, the positions of basalt liquidus curve projections can be calculated by combined solution of Eqs. (1) and (2) and the constant water pressure line equation (liquidus projection) (5) obtained by integrating the Clausius–Clapeyron relation with lower limits determined by the melting curve coordinates in accordance with t–$P_{\text{H}_2\text{O}}$ ($P_{\text{H}_2\text{O}} = P_S$):

$$P_{\text{H}_2\text{O}} = P_S - \frac{41.837(t_2 - t_1)[x(S^{liq}_{\text{H}_2\text{O}} - P_{\text{H}_2\text{O}}) + (1-x)\Delta S]}{xV^{liq}_{\text{H}_2\text{O}} + (1-x)\Delta V}, \quad (5)$$

where x is the molar fraction of water in the melt, $S^{liq}_{\text{H}_2\text{O}}$ is its partial molar entropy, $S_{\text{H}_2\text{O}}$ is water vapor molar entropy, and $V^{liq}_{\text{H}_2\text{O}}$ is the partial molar volume of water in the melt.

At $M^{liq}/M_{\text{H}_2\text{O}} = 3.555$, the relationship between the molar fraction of water in the melt (x) and its molar percentage ($N_{\text{H}_2\text{O}}$) is as follows:

$$x = \frac{3.555N_{\text{H}_2\text{O}}/(100 - N_{\text{H}_2\text{O}})}{1 + 3.555N_{\text{H}_2\text{O}}/(100 - N_{\text{H}_2\text{O}})}. \quad (6)$$

The entropy of liquid water ($S^{liq}_{\text{H}_2\text{O}}$) cannot be determined at high temperatures. However, extrapolation of available data indicates that $S^{liq}_{\text{H}_2\text{O}}$ varies almost

linearly in the temperature range 700–1200°C. Its variation is insignificant: 34.65–36.8 e.u. The $S^{liq}_{H_2O}$ and S_{H_2O} values were extrapolated in the range 1000–1200°C. For lower temperatures, they were taken from reference books [Perchuk, 1973].

The dependence of $V^{liq}_{H_2O}$ on t and P_{H_2O} is known only for albite melts [Burnham and Davis, 1971]:

$$V^{liq}_{H_2O} = 10.98 + 0.962t + 0.1005t^2 - 0.00199t^3 - 100P(0.53 + 0.2031t + 0.00158t^2) + 0.396P^3 + 100P^2(0.078 + 0.01144t), \text{ cm}^3/\text{mol}, \quad (7)$$

where t is $0.01n$ of the specified temperature in °C, and pressure is expressed in MPa. Because of the scarcity of experimental data for basic melts, $V^{liq}_{H_2O}$ values were calculated for construction of constant water pressure lines by Eq. (7).

The water-saturated liquidus curves, contour lines of water solubility in the melt, and projections of basalt liquidus curves constructed for specified P_{H_2O} values are shown in Fig. 3. It is apparent that the calculated constant water pressure lines are shifted to lower temperatures at the absence of other gaseous components. This fact reflects the dependence of $V^{liq}_{H_2O}$ on temperature, pressure, and the melt composition.

Dry solidus. Experiments indicate that partial melting of gabbro in the Ni–NiO buffer gives rise to silica-rich melts of a plagiogranite composition [Koepke et al., 2004]. The inverse problem can be solved: crystallization of a basalt sample with COMAGMAT software at P = 0.1, 0.5, and 1 GPa [Ariskin, 1999]. At the maximum crystallization level (78 wt %) in the Ni–NiO buffer, the composition of the residual melt corresponds to adamellite (Table 1). Its calculated parameters (t and $(dP/dt)^{liq}$) were used for construction of the dry solidus curve for the basalt under study.

The position of the dry solidus curve (Fig. 3) calculated for the maximum melt crystallization level matches the dry solidus curve experimentally constructed for andesite [Ishbulatov, 1977]. This fact indicates that this basalt melt is differentiated only to the andesite composition, which is confirmed by inclusions captured at final crystallization stages, whose compositions are close to those of andesite. Hence, the chosen model of *adamellite solidus* is in good agreement with the andesite solidus.

Water-saturated solidus. The water-saturated solidus curve was constructed from the constraint equations for P and t depending on N_{H_2O} [Perchuk, 1973] obtained by thermodynamic processing of data from the literature [Hamilton et al, 1964; Nesbit and Hamilton, 1970]:

$$t(^\circ\text{C}) = 1029.16 - 71.40N_{H_2O} + 5.66N^2_{H_2O} - 0.17N^3_{H_2O}, \quad (8)$$

$$P(\text{MPa}) = 100(-1015.53 + 1158.93N_{H_2O} - 74.97N^2_{H_2O} + 2.86N^3_{H_2O}), \quad (9)$$

where N_{H_2O} is water content in the melt, wt %.

For water-containing melts, we should know the projections of the contour lines of water solubility in the melt ($X^{liq}_{H_2O}$) on the liquidus and solidus and the projections of the contour lines of water content in the equilibrium fluid.

Contour lines for water solubility in the melt. At $P_{H_2O} = 0$, the line $X_{H_2O} = 0$ precisely matches the dry solidus. With the presence of water in the system, the slope of $X^{liq}_{H_2O}$ lines in the P_S–t plot should either equal or slightly exceed the slope of the dry solidus curve, because

$$\left(\frac{dP_s}{dt}\right)_{X^{liq}_{H_2O}} \approx \left(\frac{dP_s}{dt}\right)_{X^{liq}_{H_2O}=0} - \frac{R\ln(1 - X^{liq}_{H_2O}) - S^{liq}}{V^{liq} - V^{sol}}. \quad (10)$$

The second term in the right side of Eq. (10) is small but negative. Therefore, the derivative $\left(\frac{dP_s}{dt}\right)_{X^{liq}_{H_2O}}$ slightly increases with $X^{liq}_{H_2O}$. It follows from our calculations that this increment little affects the projections slopes at P_{H_2O} = const. For this reason, we assumed the condition of equal slopes of water solubility contour lines up to the case $X_{H_2O} = 0$ (Fig. 3):

$$\left(\frac{dP_s}{dt}\right)_{X^{liq}_{H_2O}} \approx \left(\frac{dP_s}{dt}\right)_{X^{liq}_{H_2O}=0} \approx 15.385 \text{ MPa}/^\circ\text{C}. \quad (11)$$

Projections of the basalt solidus curves on the P_s–t plane at specified P_{H_2O} values. It has been shown above that the adamellite model of the solidus of the basalt under study satisfactorily describes its location in the P_s–t chart, because the molecular weight, volume, and density of adamellite are close to the compositional and thermodynamic parameters of basalt *solidus* (Table 3, Fig. 3). The volume effect of adamellite melting ΔV is $V^{sol} = \Sigma X_i M_i/\rho = 24.71$; it follows that $V^{liq} - V^{sol} = \Delta V = 2.28$ cm^3. Correspondingly, the entropy effect of melting ΔS at $(dP/dt)^{liq} = 15.385$ MPa/°C is, $\Delta S = \Delta V\,(dP/dt)^{liq} = 32.125$ cm^3 MPa/°C = 8.40 e.u.

The liquidus projections at specified P_{H_2O} values were calculated by combined solution of Eqs. (8) and (9) and the constant water pressure line equation (5).

Taking into account the proximity of the properties of the andesite, adamellite, and albite melts (see above), we can apply constraint equation (7) to the calculation of $V^{liq}_{H_2O}$ and complete the calculation of the P_s–t plot in Fig. 3.

The P–T–X_{H_2O} trend. Several works have been dedicated to magma crystallization conditions in Klyuchevskoi Volcano. The trend of evolution of high-alumina basalt melt of the Apakhonchich lava flow was constructed by Mironov and Portnyagin [2008] from data on melt inclusions. Water content in melts in equilibrium with $Ol_{>82}$ (generation I) was estimated on the base of data on maximum water concentrations in melt inclusions in olivine of generation I with allowance made for water accumulation during fractionation. Water concentrations in melts in equilibrium with more iron-rich olivine (generations II and III) were calculated from the crystallization temperature difference between olivine and plagioclase. Temperatures of phenocryst mineral crystallization were evaluated by calculating pseudoliquidus values of the temperature of their equilibrium with particular melts. The melt crystallization pressure was deduced from *Cpx* composition with independent assessment from liquid CO_2 inclusions.

Estimates of P–T parameters obtained by studying melt inclusions in olivines of the three generations (Table 2) [Mironov et al., 2001; Mironov and Portnyagin, 2008] are depicted in Fig. 3. The crystallization of the parental high-magnesium basalt magmas of Klyuchevskoi Volcano began at 1250–1300°C at water concentration 3 wt % and pressure 1.05–1.2 GPa (about 37–42 km) [Mironov and Portnyagin, 2008]. These P–T parameters are outside the chart presented in Fig. 3, where the thermodynamic parameters of the water-containing basalt melt at $P > 1$ GPa are unknown because of the $X^{liq}_{H_2O}$ discontinuity at ~1.05 GPa [Perchuk, 1985].

The mean water concentration in melt inclusions in Ol_1 and Ol_2 is about 4 wt %, and in olivines of generation III (Ol_3), about 2 wt % (Table 2). The low water concentration in Ol_3 inclusions could be related to intense separation of the fluid phase (gas drainage) owing to the pressure drop during magma rise to the surface. As the ranges of P and T determinations for Ol_2 and Ol_3 overlap (Fig. 3b), the P–T plot of the melt evolution trend can be drawn to the range of their medium values. In Fig. 3, the crystallization point I of (Ol_1) with water concentration 3.9 ± 0.4 wt % is in the vicinity of the 4 wt % contour line of water solubility in the melt, i.e., near the liquidus. The degree of basalt crystallinity can be roughly assessed at this step from the locations of points II (Ol_2) and III (Ol_3). On the stretch between the liquidus and solidus contour lines with a water concentration of 4 wt %, they correspond to ~82% melt and ~18% crystalline matter (Fig. 3a). The quantitative relationships between phenocrysts and glass satisfactorily agree with the macroscopic relationships in the basalt sample under study: 35 and 65%, respectively. The amount of phenocrysts averaged over the Apakhonchich flow is about 10%.

Viscosity Calculation and Assessment of the Transport Properties of the Basalt Melt. The viscosity of basalt from the Apakhonchich flow was calculated according to Persikov's model [1984]. Without regard for the crystalline phase, it is 8×10^2 Pa/s at 1100°C, 1 GPa, and 3 wt % water. The ratio $Fe^{2+}/(Fe^{2+} + Fe^{3+})$ was estimated for viscosity calculation from chemical analyses of Apakhonchich basalts reported by Persikov [1984]. In the presence of 10% crystals, the apparent viscosity is 1.1×10^3 Pa s. Magma can rise to the surface owing to lithostatic pressure only on the condition that its density is lower than that of the surrounding rocks. According to geophysical data reported in Balesta et al. [1991], rock density in the area of the Klyuchevskoi volcano group is broadly variable. It is 2.3–2.6 g/cm^3 in upper horizons, and the mean rock density is 2.8 g/cm^3. The density of the original dry basalt melt in Klyuchevskoi Volcano is 2.75 g/cm^3, as calculated using KWareMagma software [Wohletz, 1999]. Water presence in the melt (3.3–3.4 wt %) reduces its density to 2.5 g/cm^3, thereby allowing it to ascent to the surface. The force driving magma to the surface (buoyancy) is determined by the difference between the densities of the basalt melt and the surrounding rocks. The crystallization pressure determined for Ol_1 is 0.8–1 GPa (Table 2), which corresponds to the depth of 30–35 km. With regard to this depth and calculated density, the excessive pressure that extrudes magma to the surface was calculated to be about 10 MPa.

Determination of magma ascent velocity is a complex problem. In particular, magma ascent in the channel is described by the Navier–Stokes equations, which require computer simulation. This is a task for the future.

CONCLUSIONS

Thermodynamic and rheological parameters of the basaltic melt from the Apakhonchich lava flow (Klyuchevskoi Volcano, Kamchatka) were calculated and projections of water-containing liquidus curves on the P–T plane were constructed on the base of petrologic studies and theoretical considerations. Patterns in the changes of parental melt composition and water concentration were deduced from data on melt inclusions in three olivine generations. As a result, the P–T–X_{H_2O} parameters of basalt magma formation, the degree of its differentiation, and effusion settings were determined. The location of constant water pressure lines in

the P_s–T chart indicates that the partial molar volume of water in the melt ($V^{liq}_{H_2O}$), with no other gaseous components, depends not only on P and T but also on melt composition. At $N^{liq}_{H_2O}$ = 3.3–3.4 wt % and the average crystal percentage for the Apakhonchich flow (10%), the apparent viscosity of the melt is 1.1 × 10^3 Pa s, and the density is 2.5 g/cm^3. At this density and the initial crystallization pressure, the excessive pressure, responsible for magma ascent to the surface, is about 10 MPa.

Plagioclase zoning is a special problem. The data on basalt evolution in Klyuchevskoi Volcano (deep magma formation site, polybaric fractionation with ascent, and water concentration change) suggest that the following order of events yields the observed zoning:

(1) Crystallization of the bytownite core at a large depth. The high water content, about 4 wt %, and lithostatic pressure favor stabilization of calcic plagioclase.

(2) Plagioclase dissolution with pressure decrease as magma rises.

(3) Crystallization of labradorite from the magma at lower pressures and water contents in an intermediate chamber.

The potassium contents in rocks of the Apakhonchich flow and in melt inclusions differ significantly (Tables 1 and 2). We suggest that this difference is related to an increase in the chemical potential of K_2O during melt evolution, which would affect the plagioclase composition by analogy with Korzhinskii's reaction [*Petrografiya*, 1976], where the melt plays the role of potassium feldspar:

$$Pl_{Ca–Na} + K_2O\ (\textit{in the melt}) = Pl_{Ca} + Na_2O\ (\textit{in the melt}).$$

The increase in $\mu^{liq}_{K_2O}$ should shift the equilibrium to the right to yield anorthite-enriched rims. However, studies of phenocryst zoning revealed the absence of such rims (Fig. 2), because potassium was inert during melt evolution. This fact can also be explained by Bowen's fractional crystallization, which is accompanied by potassium accumulation in the melt. It has been shown [Ariskin, 1999] that polybaric fractionation close to 40% causes significant potassium accumulation in the melt. This value is close to the percentage of phenocrysts in the basalt sample under study (35%).

ACKNOWLEDGMENTS

The back-scattered electron photographs and analyses presented in the article were made with a Jeol JSM-6480LV* scanning electron microscope with a combined EDS–WDS system at the Laboratory of Local Methods of Matter Investigation, Department of Petrology, Moscow University, under supervision of V.O. Yapaskurt, to whom the authors are grateful.

We are very grateful to Prof. L.L. Perchuk† for posing the problem and regular help in its solution and to P.Yu. Plechov for constant support and fruitful discussion. We also acknowledge the critical remarks made by the reviewers A.A. Ariskin and E.S. Persikov, which helped us to improve the manuscript.

This work was supported by the Program of the President of the Russian Federation Leading Scientific Schools, project no. 1949.2008.5.

REFERENCES

Appen, A.A., *Khimiya stekla* (The Chemistry of Glasses), Leningrad: Khimiya, 1970.

Ariskin, A.A., Phase Equilibrium Modeling in Igneous Petrology: Use of COMAGMAT Model for Simulating Fraction of Ferro-Basaltic Magmas and the Genesis of High-Alumina Basalt, *J. Volcanol. Geotherm. Res.*, 1999, vol. 90, pp. 115–162.

Balesta, S.T., Gontovaya, L.I., Kargopol'tsev, V.A., et al., Results of Seismic Investigation of the Earth Crust in the Area of Klyuchevskoi Volcano, *Vulkanol., Seismol*, 1991, no. 3, pp. 3–18.

Burnham, C.W. and Davis, N.F., The Role of H_2O in Silicate Melts. P–V–T Relations in the System $NaAlSi_3O_8$–H_2O to 1-kbar and 1000°C, *Am. J. Sci.*, 1971, vol. 270, pp. 54–79.

Dixon, J.E., Stolper, E.M., and Holloway, J.R., An Experimental Study of Water and Carbon Dioxide Solubility in Mid-Ocean Ridge Basaltic Liquids. Part I: Calibration and Solubility Models, *J. Petrol.,* 1995, vol. 36, no. 6, pp. 1607–1631.

Hamilton, D.L., Burnham, C.W., and Osborn, E.F., The Solubility of Water and Effects of Oxygen Fugacity and Water Content on Crystallization in Mafic Magmas, *J. High Resolut. Chromatogr. Chromatogr. Commun.*, 1964, vol. 5, no. 1, pp. 21–39.

Holloway, J.R., Mysen, B.O., and Eggler, D.H., *The Solubility of CO_2 in Liquids on the Joint CaO–MgO–SiO_2–CO_2*, Washington, DC: Carnegie Inst, 1976.

Ishbulatov, R.A., Experimental Study of Melting of Rocks of the Calc–Alkaline Series at 25–45 Kbar, *Ocherki Fiz-Khim. Petrol.* (Sketches of Physicochemical Petrol.), 1977, no. 7, pp. 97–168.

Izbekov, P.E., Eichelberger, J.C., Patino, L.C., et al., Calcic Cores of Plagioclase Phenocrysts in Andesite from Karymsky Volcano: Evidence for Rapid Introduction by Basaltic Replenishment, *Geol.*, 2002, vol. 30, no. 9, pp. 799–802.

Kadik, A.A., Lebedev, E.B., and Khitarov, N.I., *Voda v magmaticheskikh rasplavakh* (Water in Magmatic Melts), Moscow: Nauka, 1971.

Koepke, J., Feig, S.T., Snow, J., and Freise, M., Petrogenesis of Oceanic Plagiogranite by Partial Melting of Gabbros: An Experimental Study, *Contrib. Mineral. Petrol.*, 2004, vol. 146, no. 4, pp. 414–432.

† Deceased.

Mironov, N.L. and Portnyagin, M.V., Dynamics of Crystallization and Magma Transport in Klyuchevskoi Volcano (Kamchatka), in *XIII Vseros. konf. po termobarogeokhimii* (XIII All-Russia Conference on Thermobarogeochemistry), Moscow: IGEM RAN, 2008.

Mironov, N.L., Portnyagin, M.V., Plechov, P.Yu., and Khubunaya, S.A., Final Stages in Evolution of Magmas of Klyuchevskoi Volcano from Studies of Melt Inclusions in Minerals of High-Alumina Basalts, *Petrologiya*, 2001, no. 1, pp. 51–69 [*Petrology* (Engl. Transl.), no. 1, pp. 46–63].

Mysen, B.O., *Volatiles in Magmatic Liquids, Prog. Metam. Magm. Petrol,* Cambridge: Univ. Press, 2004, pp. 435–475.

Nesbit, R.W. and Hamilton, D.L., Crystallization of Alkali-Olivine Basalts under Controlled P_{O_2}, P_{H_2O} Conditions, *Phys. Earth and Planet. Int.*, 1970, vol. 3, p. 309.

Perchuk, L.L., *Termodinamicheskii rezhim glubinnogo petrogeneza* (Thermodynamics of Deep-Seated Petrogenesis), Moscow: Nauka, 1973.

Perchuk, L.L., Pressure Dependence of Basalt Liquidus Temperature in Dry Systems, *Dokl. Akad. Nauk SSSR*, 1983, vol. 271, no. 3, pp. 702–705.

Perchuk, L.L., Alkaline Basalt–Water System, 2. Liquidus Surface within a Pressure Range of 1 bar–20 kbar, *Ocherki Fiz.-Khim. Petrol.* (Sketches in Physicochemical Petrol.), 1985, no. 13, pp. 60–80.

Persikov, E.S., The Viscosity of Magmatic Liquids: Experiment, Generalized Patterns; a Model for Calculation and Prediction; Application, Physical Chemistry of Magmas, *Adv. Phys. Geochem.*, New York: Springer, 1991, vol. 9, pp. 1–40.

Persikov, E.S., *Vyazkost' magmaticheskikh rasplavov* (Viscosity of Magmatic Melts), Moscow: Nauka, 1984.

Petrografiya (Petrography), Moscow: Izd. Mosk. Univ., 1976, vol. 1.

Silver, L. and Stolper, E., A Thermodynamic Model for Hydrous Silicate Melts, *J. Geol.*, 1985, vol. 93, pp. 161–178.

Vance, J., Zoning in Igneous Plagioclase: Patchy Zoning, *J. High Resolut. Chromatogr. Chromatogr. Commun.,* 1965, vol. 73, pp. 636–651.

Wohletz, K.H., MAGMA: Calculates IUGS Volcanic Rock Classification, Densities, and Viscosities, *Los Alamos Nat. Lab. Comp. Code*, LA-: CC 99-28. New Mexico, 1999.